NJC

New Journal of Chemistry

A journal for new directions in chemistry

Accepted Manuscript

This article can be cited before page numbers have been issued, to do this please use: M. Madni, M. N. Ahmed, M. Hafeez, M. Ashfaq, M. N. Tahir, D. M. Gil, B. Galmes, S. Hameed and A. Frontera, *New J. Chem.*, 2020, DOI: 10.1039/D0NJ02931A.

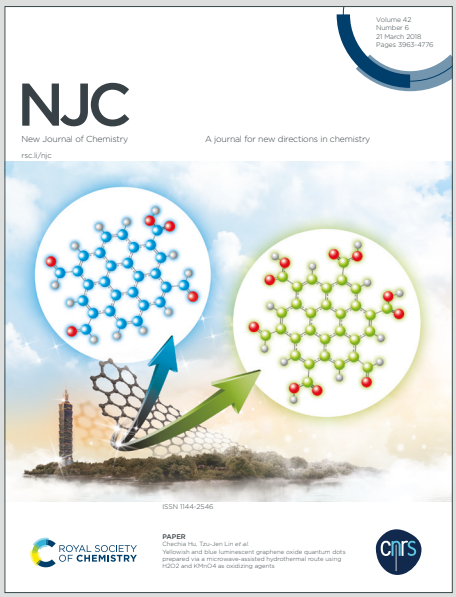

This is an Accepted Manuscript, which has been through the Royal Society of Chemistry peer review process and has been accepted for publication.

Accepted Manuscripts are published online shortly after acceptance, before technical editing, formatting and proof reading. Using this free service, authors can make their results available to the community, in citable form, before we publish the edited article. We will replace this Accepted Manuscript with the edited and formatted Advance Article as soon as it is available.

You can find more information about Accepted Manuscripts in the Information for Authors.

Please note that technical editing may introduce minor changes to the text and/or graphics, which may alter content. The journal's standard Terms & Conditions and the Ethical guidelines still apply. In no event shall the Royal Society of Chemistry be held responsible for any errors or omissions in this Accepted Manuscript or any consequences arising from the use of any information it contains.

Journal Name

ROYAL SOCIETY OF CHEMISTRY View Article Online
DOI: 10.1039/D0NJ02931A

ARTICLE

Recurrent π–π stacking motifs in three new 4,5-dihydropyrazolyl-thiazole-coumarin hybrids: X-ray characterization, Hirshfeld surface analysis and DFT calculations

Received 00th January 20xx,
Accepted 00th January 20xx

DOI:

www.rsc.org/

Murtaza Madni[a], Muhammad Naeem Ahmed[b]*, Muhammad Hafeez[b], Muhammad Ashfaq[c], Muhammad Nawaz Tahir[c], Diego M. Gil,[d] Bartomeu Galmés[e], Shahid Hameed[a]*, and Antonio Frontera[e,]*

The synthesis and X-ray characterization of three new 4,5-dihydropyrazolylthiazole-coumarin hybrids (**1-3**) are reported herein, namely 3-(2-(3,5-bis(4-chlorophenyl)-4,5-dihydropyrazol-1-yl)thiazol-4-yl)-2*H*-chromen-2-one (**1**), 3-(2-(5-(4-chlorophenyl)-4,5-dihydro-3-phenylpyrazol-1-yl)thiazol-4-yl)-2*H*-chromen-2-one (**2**) and 3-(2-(3-(4-Chlorophenyl)-4,5-dihydro-5-*p*-tolylpyrazol-1-yl)thiazol-4-yl)-2*H*-chromen-2-one (**3**). A detailed structural analysis of the noncovalent interactions and their evaluation using Hirshfeld surface analysis is also reported, evidencing the importance of C–H···O and π–π interactions. Finally, DFT calculations along with the molecular electrostatic potential (MEP) and NCIplot index analysis have been used to evaluate those interactions energetically and to investigate the relative importance of two different π-stacking modes that are recurrent binding motifs in the solid state architecture of the three complexes.

1. Introduction

Owing to numerous pharmacological and biological applications thiazole derivatives have gained tremendous attention in the scientific community. Thiazole is reported in literature as antibacterial,[1] antiviral,[2] anti-inflammatory,[3] antifungal,[4] antitubercular,[5] antitumoral,[6] anti-HIV[7] and antioxidant agent.[8] Moreover, numerous marketed drugs possess thiazole scaffold as an active group.[9] Besides thiazole, pyrazoline ring is also biologically valuable structural motif. Recently, various pyrazoline containing compounds e.g. kebuzone, mefobutazone, phenylbutazone[10] and ramifenazone[11] are found to have potent anti-inflammatory activity. Moreover, pyrazoline derivatives exhibit many pharmaceutical effects such as antitumor,[12] antibacterial,[13] antifungal[14] and antidepressant[15] activities.

Coumarin moiety is also an important structural motif of many antibiotics. Moreover, in the literature antibacterial activity of coumarins against Gram-positive bacteria is also reported.[16-18] Dicoumarol and warfarin contain coumarin ring and are utilized as anticoagulant of blood in different organs (veins, lungs and heart) of living beings.[19] Coumarin has diverse biological applications like anti-HIV,[20] anticonvulsant,[21] antihyperglycemic,[22] antioxidant,[23] antifungal,[24] and anticancer.[25] Apart from the pharmacological properties,[26] substituted coumarin derivatives also find applications in dyes due to their unique optical and photophysical properties.[27] Coumarin-thiazoles based dyes are used as fluorescence labels,[28] optical brighteners,[29] non-linear optical materials,[30] solar energy absorbers, laser dyes and as two-photon absorption (TPA) materials.[31] 3-Substituted pyrazolyl thiazolyl based coumarin dyes have also been used as fluorescent brightening agents,[32] red, green and blue dopants in organic light-emitting diodes.[33]

We have recently analysed the importance of antiparallel π–π interactions in isatin bases hidrazines[34] and π-hole tetrel bonding[35] in 2-triazolyl-2-oxoacetate derivatives. Herein, in this new investigation, we report the synthesis and X-ray characterization of three new 4,5-dihydropyrazolyl-thiazole-coumarin hybrids that present almost coplanar 4,5-dihydropyrazole, thiazole and coumarin rings, thus having an extended π-surface that strongly influence their solid state architecture. Several types of π-stacking motifs are found, which have been studied using Hirshfeld surface analysis and DFT calculations. Uncommon 4,5-dihydropyrazole···thiazole stacking interactions between aromatic and aliphatic rings are also described and studied. This type of stacking between heteroaromatic and heteroaliphatic five membered rings has not been studied before, as far as our knowledge extends. Conventional and well-accepted stacking interactions frequently occur between organic aromatic molecules or

[a] Department of Chemistry, Quaid-i-Azam University, Islamabad 45320, Pakistan
[b] Department of Chemistry, The University of Azad Jammu and Kashmir, Muzaffarabad, 13100 Pakistan
[c] Department of Physics, University of Sargodha, Sargodha, Pakistan
[d] INBIOFAL (CONICET - UNT), Instituto de Química Orgánica - Cátedra de Química Orgánica I, Facultad de Bioquímica, Química y Farmacia, Universidad Nacional de Tucumán, Ayacucho 471 (T4000INI), San Miguel de Tucumán - Tucumán – Argentina
[e] Department de Quimica, Universitat de les Illes Balears, Crta. De Valldemossa km 7.5, 07122 Palma de Mallorca (Baleares), Spains

*CCDC 981487, 1009298 and 1009300 contain the supplementary crystallographic data for compounds **1, 2** and **3**, respectively.*

fragments. However, a variety of fragments[36] can also be involved in stacking interactions, like chelate rings,[37] yielding to complexes that are usually stronger than stacking between benzene molecules.[37,38] Theoretical calculations combined with statistical analysis of the Cambridge Structural Database have been used to analyse[39] the geometric and energetic features of the interaction between benzene and cyclohexane that, remarkably, is stronger than either the benzene dimer, or the cyclohexane dimer (−2.62 kcal/mol).[40]

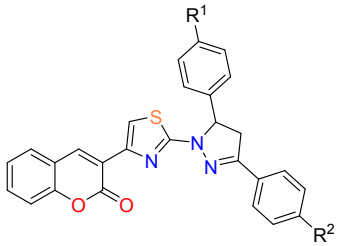

1, $R^1 = R^2 = Cl$
2, R^1 =Cl, R^2 = H
3, $R^1 = CH_3$, R^2 = Cl

Scheme 1. A Compounds **1-3** synthesized in this work.

2. Experimental

2.1. Synthesis

Compounds **1-3** were synthesized by following a procedure already reported in literature[26,41] with slight modification. A 2-neck round bottom flask was charged with substituted chacones, thiosemicarbazide and sodium hydroxide in ethanol. The reaction mixture was refluxed to get 3, 5-disubstituted phenyl-4, 5-dihydropyrazole-1-carbothioamide. Finally, 3,5-disubstituted phenyl-4, 5-dihydropyrazole-1-carbothioamide was added to a suspension of 3-(2-bromoacetyl)-2*H*-chromen-2-one in ethanol and stirred vigorously under reflux for 2 hours to get the desired compounds (**1-3**) Scheme 2.

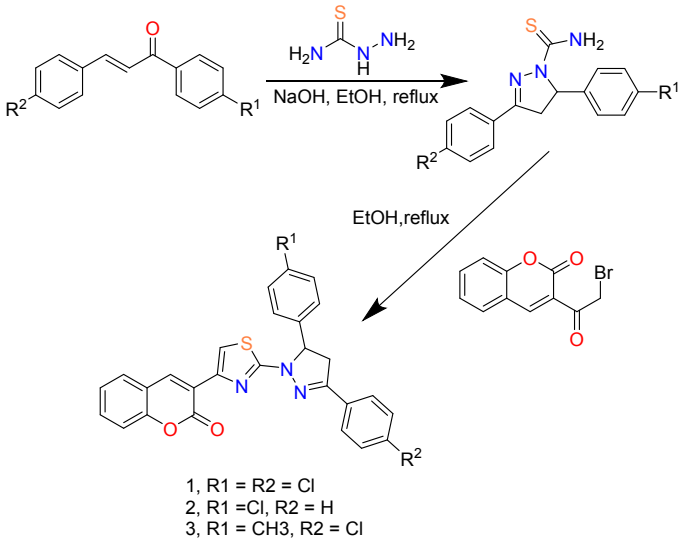

1, R1 = R2 = Cl
2, R1 =Cl, R2 = H
3, R1 = CH3, R2 = Cl

Scheme 2: Synthetic route for the target compounds (**1-3**).

3-(2-(3,5-Bis(4-chlorophenyl)-4,5-dihydropyrazol-1-yl)thiazol-4-yl)-2*H*-chromen-2-one (1)

View Article Online
DOI: 10.1039/D0NJ02931A

Pale yellow solid; **Yield**: 81%; **m.p.:** 249˚C; R_f = 0.49 (chloroform: acetone, 9:1); **IR (ν,** neat, cm^{-1}**):** 1723 (C=O), 2903 (C-H), 3143 (C=C-H); **^{1}H-NMR** (300 MHz, $CDCl_3$)**: δ** 3.29 (1H, dd, J_{cis} = 7.5Hz, J_{gem} = 17.4Hz, CH-pyrazoline), 3.91 (1H, dd, J_{trans} = 12Hz, J_{gem} = 17.4Hz, CH-pyrazoline), 5.61 (1H, dd, J_{cis} = 7.5Hz, J_{trans} = 12Hz, CH-pyrazoline), 7.27-7.85 (13H, m, Ar), 8.13 (1H, s, CH-thiazole); **^{13}C-NMR** (75 MHz, $CDCl_3$)**: δ** 43.42, 64.52, 111.91, 116.28, 119.63, 121.13, 124.44, 127.58, 128.01, 128.13, 128.96, 129.04, 129.65, 131.08, 133.67, 135.96, 138.57, 140.06, 144.40, 150.68, 152.78, 159.63, 163.92;); HRMS (EI-TOF) [M^+] Calcd. for: $C_{27}H_{17}Cl_2N_3O_2S$: 518.414; found; 518.416.

3-(2-(5-(4-chlorophenyl)-4,5-dihydro-3-phenylpyrazol-1-yl)thiazol-4-yl)-2H-chromen-2-one (2)

Pale yellow solid; **Yield**: 87%; **m.p.:** 199˚C; R_f = 0.50 (chloroform: acetone, 9:1); **IR (ν ,** neat, cm^{-1}**):** 1708 (C=O), 2921 (C-H), 3136 (C=C-H); **^{1}H-NMR** (300 MHz, $CDCl_3$)**: δ** 3.32 (1H, dd, J_{cis} = 7.5Hz, J_{gem} = 17.4Hz, C^4H-pyrazoline), 3.94 (1H, dd, J_{trans} = 12Hz, J_{gem} = 17.4Hz, CH-pyrazoline), 5.60 (1H, dd, J_{cis} = 7.5Hz, J_{trans} = 12Hz, CH-pyrazoline), 7.26-7.84 (14H, m, Ar), 8.14 (1H, s, CH-thiazole); **^{13}C-NMR** (75 MHz, $CDCl_3$)**: δ** 43.56, 64.38, 111.83, 116.26, 119.68, 121.18, 124.42, 126.41, 128.06, 128.13, 128.77, 128.91, 130.05, 131.01, 131.14, 133.57, 138.50, 140.29, 144.37, 151.87, 152.78, 159.64, 164.12;); HRMS (EI-TOF) [M^+] Calcd. for: $C_{26}H_{30}N_4O_5S_2$: 542.1658; found; 542.1656.

3-(2-(3-(4-Chlorophenyl)-4,5-dihydro-5-p-tolylpyrazol-1-yl)thiazol-4-yl)-2*H*-chromen-2-one (3)

Pale yellow solid; **Yield**: 88%; **m.p.:** 250˚C; R_f = 0.52 R_f = 0.45 (chloroform: acetone, 9:1); **IR (ν ,** neat, cm^{-1}**):** 1709(C=O), 2934 (C-H), 3128 (C=C-H); **^{1}H-NMR** (300 MHz, $CDCl_3$)**: δ** 2.35 (3H, s, CH_3), 3.32 (1H, dd, J_{cis} = 7.2Hz, J_{gem} = 17.4Hz, CH-pyrazoline), 3.89 (1H, dd, J_{trans} = 12Hz, J_{gem} = 17.4Hz, CH-pyrazoline), 5.61 (1H, dd, J_{cis} = 7.2Hz, J_{trans} = 12Hz, CH-pyrazoline), 7.19-8.21(13H, m, Ar), 8.64 (1H, s, CH-thiazole); **^{13}C-NMR** (75 MHz, $CDCl_3$)**: δ** 21.18, 43.49, 64.84, 111.69, 116.28, 119.73, 121.19, 124.38, 126.59, 127.58, 128.08, 128.98, 129.43, 129.91, 130.44, 130.98, 137.66, 138.55, 138.60, 144.39, 150.74, 152.76, 159.65, 163.91;); HRMS (EI-TOF) [M^+] Calcd. for: $C_{28}H_{20}ClN_3O_2S$: 497.995; found; 497.994.

2.2. Instrumentation

Compounds **1-3** were synthesized by following a procedure already reported in literature[26,41] and were mainly characterized by IR, NMR and single crystal X-ray crystallography. Melting points were determined on a Yanaco melting point apparatus and are reported as uncorrected. FT-IR spectra were recorded on Thermoscientific Fourier Transform Infra-Red Spectrophotometer USA model nicolet 6700 using Attenuated total reflectance (ATR) facility. NMR spectra were acquired on a Bruker Avance 300 MHz spectrophotometer in $CDCl_3$ solution. Chemical shifts (δ) are reported in ppm downfield from TMS. Chemical shifts were

View Article Online
DOI: 10.1039/D0NJ02974A

calibrated relative to residual solvent signal. HRMS were obtained on a Bruker microTOF-QII spectrometer.

Table 1: X-ray details of compounds **1–3**

Crystal data	1	2	3
CCDC	981487	1009298	1009300
Chemical formula	$C_{27}H_{17}Cl_2N_3O_2S$	$C_{27}H_{18}ClN_3O_2S$	$C_{28}H_{20}ClN_3O_2S$
M_r	518.40	483.95	497.98
Crystal system, space group	Triclinic, *P-1*	Monoclinic, $P2_1/c$	Triclinic, *P-1*
Temperature (K)	296	296	296
a (Å)	8.6740(6)	8.5233(9)	10.287(1)
b (Å)	11.8234(8)	22.329(3)	10.938(2)
c (Å)	12.4070(7)	12.3340(12)	11.3049 (10)
α (°)	71.363(2)	90	97.749(5)
β (°)	73.094(3)	106.201(4)	100.075(4)
γ (°)	82.970(3)	90	101.222(5)
V (Å^3)	1152.98(13)	2254.1(4)	1209.6(3)
Z	2	4	2
Density (calculated)	1.493 mg/m^3	1.426 mg/m^3	1.367 mg/m^3
F(000)	532	1000	516
Radiation type	Mo *K*α	Mo *K*α	Mo *K*α
Wavelength (λ)	0.71073 Å	0.71073 Å	0.71073 Å
μ (mm^{-1})	0.41	0.29	0.28
Crystal shape	Prism	Plate	Needle
Crystal Colour	Light yellow	Light Yellow	Yellow
Crystal size (mm)	0.38×0.26×0.24	0.35×0.28×0.20	0.37×0.23×0.21
No. of measured, independent And observed [*I*> 2s(*I*)] reflections	18290, 5105, 4262	21473, 5931, 3830	19111, 5203, 2614
R_{int}	0.025	0.051	0.041
Theta range for data collection	1.798 to 27.271°	1.824 to 27.425°	1.856 to 27.000°
Index ranges	-11≤ h ≤11, -15≤ k ≤15, -15 ≤ l ≤15	-9≤ h ≤11, -27≤ k ≤28, -15 ≤ l ≤15	-13≤ h ≤13, -12≤ k ≤13, -14 ≤ l ≤14
$(\sin\theta/\lambda)_{max}$ (Å^{-1})	0.645	0.648	0.639
$R[F^2> 2\sigma(F^2)]$, $wR(F^2)$, *S*	0.039, 0.107, 1.05	0.051, 0.127, 1.00	0.053, 0.145, 1.01
No. of reflections	5105	5071	5203
No. of parameters	316	307	317
$\Delta\rho_{max}$, $\Delta\rho_{min}$ (e Å^{-3})	0.48, −0.59	0.21, −0.33	0.28, −0.34

2.3. Crystal data and structure refinement.

The single crystal x-ray diffraction computation of compounds (**1-3**) were performed on Bruker Kappa APEXII CCD X-ray diffractometer having graphite monochromated Mo-Kα radiation (λ = 0.71073 Å). The prism, plate and needle shaped single crystals of (**1-3**), respectively appropriate for X-ray investigation were acquired from EtOH/EtOAc and placed on a glass fiber in order to collect data on Bruker Apex-II software.[42] The structures were solved effectively with the help of direct methods and subsequent difference fourier maps on SHELXS97[43] and then refined on the square of atomic factors by a full-matrix least-squares procedure utilizing anisotropic displacement parameters. H-atoms in all three structures were sited in ideal positions and refined as riding atoms with relative isotropic displacement parameters. All refinements were carried out by utilizing SHELXL-2018/3 and WinGX-2014.1 programs.[44,45] The method to collect data was ω-scans and data integration were performed using Bruker SAINT[46] software package. Data were corrected for Lorentz and polarisation effects and for absorption by SADABS. The crystallographic illustrations for the structures were prepared by utilizing ORTEP-3.[45] Experimental parameters related to single-crystal X-ray inspection of compounds are given in Table 1.

2.4. Hirshfeld surface calculations

Hirshfeld surfaces and the associated 2D fingerprint plots[47-51] were generated using the CrystalExplorer17 software.[52] The normalized contact distance (d_{norm}) based on both d_e and d_i, and the van der Waals (vdW) radii of the atoms (eq. 1) enables identification of regions involved in the main intermolecular interactions.[47,53] The value of d_{norm} is negative or positive when contacts are shorter or longer than the vdW separations, respectively. Hirshfeld surfaces of the structures were also mapped with the shape index and curvedness properties. The d_{norm} surfaces were mapped over a fixed color scale of -0.025 (red) to 0.75 (blue), shape index mapped in the color range of -1.0 au (concave) to 1.0 au (convex) and curvedness in the range -4.0 au (flat) to 0.01 au (singular).

$$d_{\text{norm}} = \frac{d_i - r_i^{vdW}}{r_i^{vdW}} + \frac{d_e - r_e^{vdW}}{r_e^{vdW}} \qquad (1)$$

The combination of d_e and d_i in the form of 2D fingerprint plots provides decomposition of Hirshfeld surfaces into relative contribution of different intermolecular interactions present in the crystal.[53] The 2D fingerprint plots were plotted by using the translated 0.6-2.6 Å range and including reciprocal contacts.

2.5. Theoretical methods

The BSSE[54] corrected energies were computed using the Turbomole 7.0 program[55] at the M06-2X[56]–D3[57]/def2-TZVP[58] level of theory and using the crystallographic coordinates. The formation energies of the assemblies were evaluated by calculating the difference between the total energy of the assembly and the sum of the monomers that constitute the assembly, which were kept frozen. This methodology has been previously used in the literature.[59] The molecular electrostatic potential was computed at the same level of theory and plotted onto the 0.001 a.u. isosurface. The NCIplot[60] isosurfaces have been used to characterize non-covalent interactions. They correspond to both favourable and unfavourable interactions, as differentiated by the sign of the second density Hessian eigenvalue and defined by the isosurface colour. The colour scheme is a red-yellow-green-blue scale with red for ρ^+_{cut} (repulsive) and blue for ρ^-_{cut} (attractive).

3. Results and discussion

3.1. Description of crystal structures

ORTEP plots of the solid state structures of compounds **1-3** are displayed in Figs. 1-3 and their X-ray geometrical parameters such as bond lengths and angles are shown in Table 2.

Compound **1** crystallized in the triclinic *P-1* space group with Z= 2 molecules per unit cell. The crystallographic results shown in Table 2 reveal that the C12-N1 and C21-N3 bond lengths are 1.294(2) and 1.284(2) Å, indicating a double bond character of these bonds. The C10-N1 and C12-N2 bond lengths are 1.395(2) and 1.357(2) Å, respectively which are considerably shorter than that expected for a single C(sp^2)-N(sp^2) bond length, with an average value of 1.472(5) Å. These observations are attributed to the importance of the resonance forms in this structure involving the N1 and N2 atoms. As shown in Fig. 1a, 2H-chromen-2-one moiety A (C1-C9/O1/O2), thiazole ring B (C10-C12/N1/S1), 4,5-dihydro-1H-pyrazole ring C (C13/C20/C21/N2/N3), chlorobenzene moieties D (C14-19/CL1) and E (C22-C27/CL2) are planar with r.m.s deviation of 0.0031, 0.0019, 0.0698, 0.0034 and 0.0043 Å, respectively. The dihedral angle between A/B, A/C, A/D, A/E, B/C, B/D, B/E, C/D, C/E and D/E are 5.2(8)°, 8.09(9)°, 86.02(3)°, 14.5(7)°, 7.06(1)°, 80.98(4)°, 19.53(9)°, 83.6(4)°, 19.5(9)° and 79.51(4)°, respectively. These dihedral angles show that the 2H-chromen-2-one moiety A and thiazole ring B are almost parallel to each other whereas the 4,5-dihydro-1H-pyrazole ring C and chlorobenzene moiety D are almost perpendicular to each other.

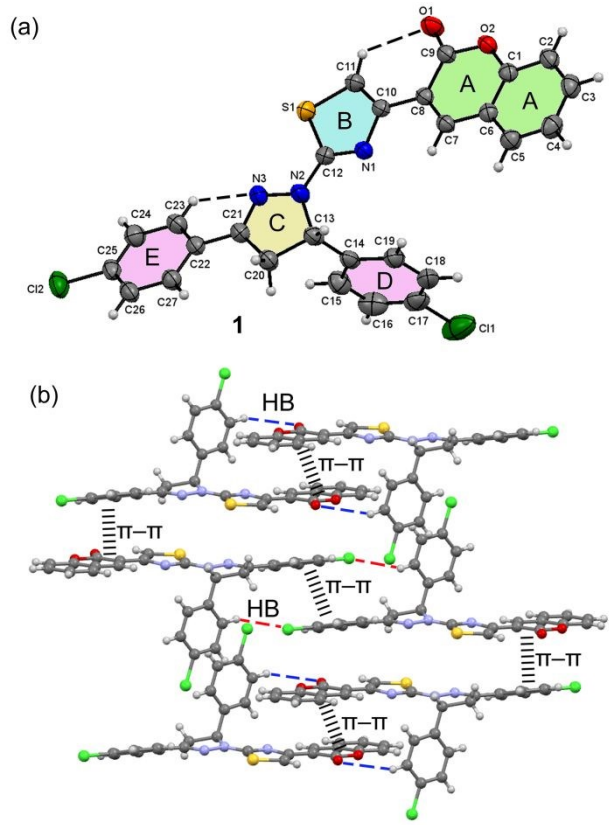

Fig. 1 (a) ORTEP diagram of **1** drawn at the probability level of 50%. H-atoms are shown by small circles of arbitrary radii. (b) X-ray packing diagram of **1** showing formation of H-bonding and π–π stacking interactions.

In the crystal packing of **1**, the molecules are linked via non-classical C16-H16···O2 and C19-H19···Cl2 hydrogen bonds (Table 3, Fig. 1b, red and blue dashed lines). The supramolecular assembly also includes the existence of three intermolecular π···π interactions (Table 4 and Fig 1b). The shorter contact involves the 2H-chromen-2-one (Cg3 centroid) rings, with d(Cg3···Cg3) = 3.4584(2) Å indicating the stronger π-stacking interaction. These interactions are further analysed below. In addition, Cg1···Cg4 and Cg3···Cg6 π-stacking interactions are also responsible of the crystal stabilization. The centroid of the chlorobenzene ring (centroid Cg5) is in contact with the O1 of the 2H-chromen-2-one moiety through lone pair···π interaction. The distance between O1 and the centroid of the π-face is 3.841 Å [angle α(C1-O1···Cg5) = 100.7°]. The shorter separation O1···C16 of 3.114 Å and the value of the angle α show significant lone pair···π interactions.[51] Additional stabilization is contributed by C-H···π interactions involved the H2 atom and the chlorobenzene ring (Cg5 centroid) to form C2-H2···Cg5 interactions [d(H2···Cg5)= 2.83 Å and <(C2-H2···Cg5)= 160°, symmetry: -x,1-y, 1-z].

Table 2. Selected geometrical parameters of compounds **1-3** (Å, °).

Parameters	**1**	**2**	**3**
C10-N1	1.395(2)	1.390(3)	1.390(3)
C12-N1	1.295(2)	1.297(3)	1.297(4)
C12-N2	1.357(2)	1.354(3)	1.354(4)
N2-N3	1.380(2)	1.387(3)	1.380(3)
C21-N3	1.284(2)	1.287(3)	-
C13-N2	1.476(3)	1.476(4)	1.463(3)
C21-C22	1.460(2)	1.461(3)	-
C22-C23	-	-	1.463(4)
C10-C8	1.465(2)	1.472(3)	-
C10-C8-C7	121.3(1)	121.1(2)	122.6(2)
N3-N2-C12	119.8(2)	119.9(2)	118.6(2)
N2-C13-C14	111.4(1)	111.8(2)	113.0(2)
N3-C21-C22	121.4(2)	121.2(2)	-

Table 3. Hydrogen bond geometrical parameters (Å, °) for compounds **1-3**.

D-H···A	d(D···H)	d(H···A)	d(D···A)	< (D-H···A)
Compound 1				
C16-H16···O2^{i}	0.93	2.99	3.725(3)	136
C19-H19···Cl2^{ii}	0.93	2.83	3.598(3)	140
Compound 2				
C18-H18···O1^{iii}	0.93	2.69	3.502(3)	146
Compound 3				
C11-H11···O1^{iv}	0.93	2.50	3.2462(6)	137
C21-H21B···O1^{v}	0.97	2.28	3.1902(6)	156
C24-H24···O1^{vi}	0.93	2.92	3.753(3)	150

Symmetry codes: (i) –x,-y+1,-z+1, (ii) –x+a,-y+2,-z-1, (iii) –x,+y+1/2,-z+1/2+1, (iv) 1-x,1-y,-z, (v) x,-1+y,z, (vi) x,y-1, z.

Compound **2** crystallizes in the monoclinic $P2_1/c$ space group, with Z= 4 molecules per unit cell. In this compound, the 2H-chromen-2-one moiety A (C1-C9/O1/O2), thiazole ring B (C10-C12/N1/S1), 4,5-dihydro-1H-pyrazole ring C (C13/C20/C21/N2/N3), chlorobenzene moiety D (C14-19/CL1) and benzene ring E (C22-C27) are planar with r.m.s deviation

View Article Online
DOI: 10.1039/D0NJ02031A

of 0.0021, 0.0012, 0.0568, 0.0083 and 0.0050 Å, respectively. The dihedral angle between A/B, A/C, A/D, A/E, B/C, B/D, B/E, C/D, C/E and D/E is 3.7(1)°, 8.41(1)°, 86.9(4)°, 10.6(1)°, 5.32(2)°, 84.93(6)°, 12.42(2)°, 85.81(6)°, 13.1(2)° and 82.69(6)°, respectively. These dihedral angles show that the 2H-chromen-2-one moiety A and thiazole ring B are almost parallel to each other. The crystal structure stabilization of **2** is supported by weak C18-H18···O1 hydrogen bonding interactions [d(H18···O1) = 2.69 Å, d(C18···O1) = 3.502(3) Å and <(C18-H18···O1) = 146°) resulting in infinite chains along the *c* axis (see Fig. 2b). These chains are further stabilized by π-stacking interactions between adjacent rings, with centroid to centroid distances between 3.4497(5) and 3.7713(5) Å (see Table 4). In addition, the crystal packing of **2** is also stabilized by C-H···π interactions (see Fig. 2c) involving the H2 atom and the chlorobenzene ring (centroid Cg5), with d(H2···Cg5) = 2.76 Å and <(C2-H2···Cg5)= 160°, symmetry: -x,-y, 1-z]. In the theoretical section below both interactions are further studied and characterized.

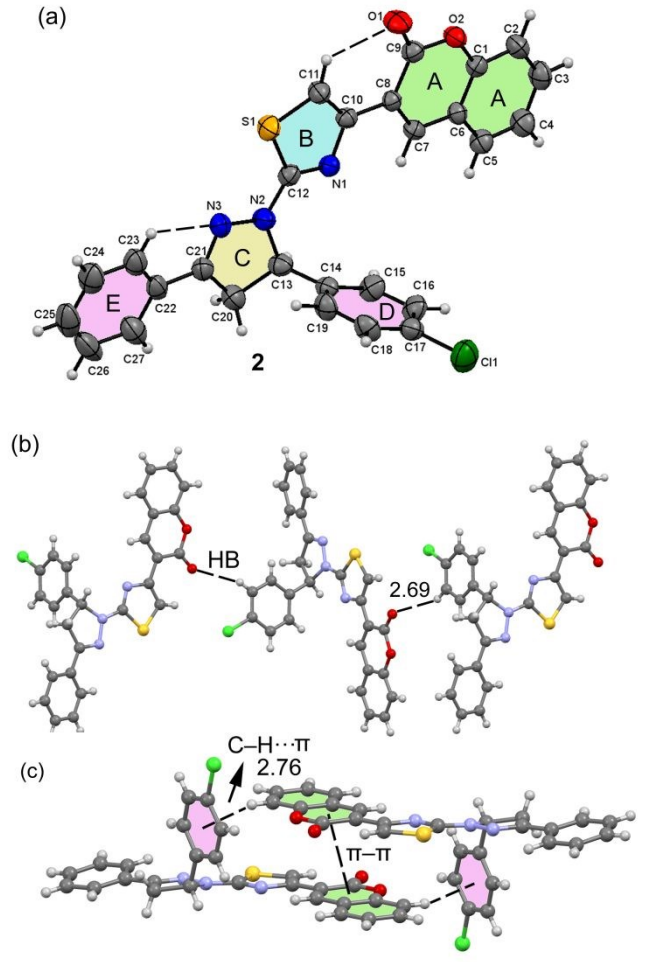

Fig. 2 (a) ORTEP diagram of **2** drawn at the probability level of 50%. H-atoms are shown by small circles of arbitrary radii. (b) Packing diagram of 2 showing formation of C–H···O bonds (c) Packing diagram of 2 showing formation of C–H···π and π–π interactions.

The crystal structure of **3** reveals that it crystallizes in the triclinic *P*-1 space group, with Z= 2 molecules per unit cell. Table 2 includes selected bond lengths and angles derived from the structural refinement. The geometrical parameters obtained for **3** are very similar to those observed for compounds **1** and **2** (see Table 2). In **3**, 2H-chromen-2-one moiety A (C1-C9/O1/O2), thiazole ring B (C10-C12/N1/S1), 4,5-dihydro-1H-pyrazole ring C (C13/C21/C22/N2/N3), toluene moiety D (C14-C20) and chlorobenzene ring E (C23-C28/CL1) are planar with r.m.s deviation of 0.0201, 0.0035, 0.0051, 0.0102 and 0.0049 Å, respectively. The dihedral angle between A/B, A/C, A/D, A/E, B/C, B/D, B/E, C/D, C/E and D/E is 9.5(1)°, 4.9(2)°, 75.7(2)°, 7.45(1)°, 8.55(2)°, 83.1(8)°, 16.7(1)°, 74.6(9)°, 11.42(2)° and 71.73(8)°, respectively.

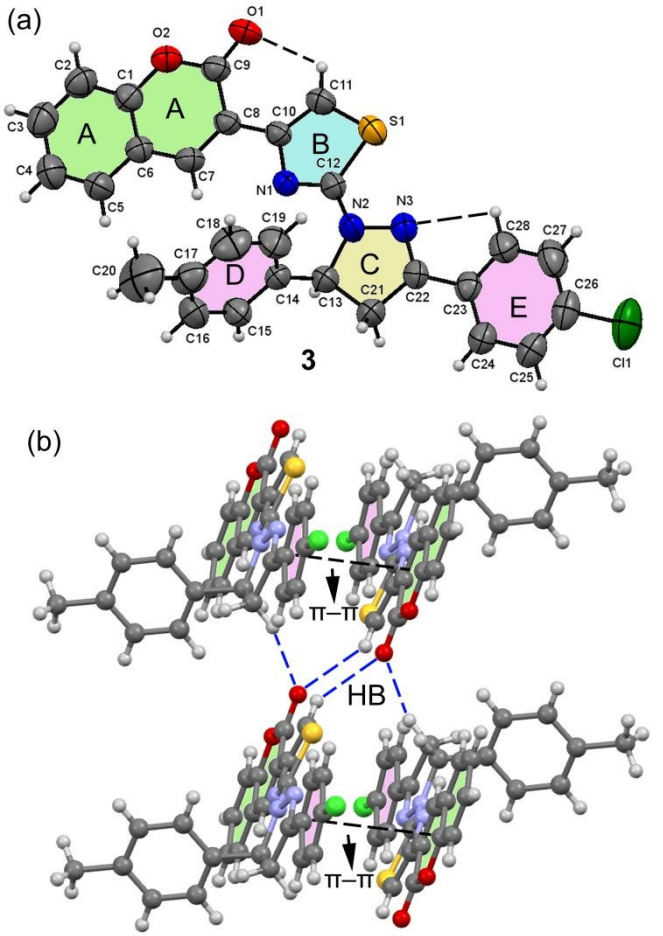

Fig. 3 (a) ORETP diagram of 3 drawn at the probability level of 50%. H-atoms are shown by small circles of arbitrary radii. (b) Packing diagram of showing dimerization of molecules with H-atoms and π-stacking interactions.

The molecules are connected with each other through C11-H11···O1 hydrogen bonds into centre-symmetric dimers stacked, giving $R_2^2(12)$ graph-set motif, as shown Fig. 3b. The crystal packing of **3** is also stabilized by weak C21-H21B···O1 hydrogen bonds involving the acceptor O1 oxygen atom from the carbonyl group and the H21B atom of the methylene

View Article Online
DOI: 10.1039/D0NJ02571A

group from the 4,5-dihydro-1H-pyrazole ring as donor. Additionally, the H24 atoms of the chlorobenzene ring are involved in intermolecular hydrogen bonds to the O1 atom from the carbonyl group to form C24-H24···O1 with H24···O1 distance of 2.92 Å (see blue dashed lines in Fig. 3b). The structure of **3** shows π···π stacking interactions with Cg3···Cg6 and Cg1···Cg2 intercentroid distances of 3.6510(7) and 3.8770(7) Å, respectively. The crystal packing of **3** also shows intermolecular C-H···π interactions involving the methylbenzene ring (centroid Cg5) and the H2 atom of the 2H-chromen-2-one moiety.

Table 4. Geometrical parameters for the π-stacking moieties involved in the π···π interactions in compounds **1-3** (Å, º).

Rings (I)-(J)[a]	Rc[b]	R1v[c]	R2v[d]	α[e]	β[f]	γ[g]
Compound **1**						
Cg1···Cg4[i]	3.6980(3)	3.3479	3.4322	5.0	21.9	25.1
Cg3···Cg3[i]	3.4584(2)	3.3373	3.3373	0.0	15.2	15.2
Cg3···Cg5[i]	5.1589(4)	0.1165	4.0905	86	37.5	88.7
Cg3···Cg6[ii]	3.6838(3)	3.4272	3.5844	14	13.3	21.5
Compound **2**						
Cg3···Cg6[iii]	3.5560(5)	3.3997	3.4944	10	10.7	17.0
Cg3···Cg3[iii]	3.4497(5)	3.3494	3.3494	0.0	13.8	13.0
Cg1···Cg4[iv]	3.7619(5)	3.4643	3.4461	4.0	23.6	22.9
Cg1···Cg2[iii]	3.7713(5)	3.6020	3.6891	5.0	12.0	17.2
Compound **3**						
Cg3···Cg6[v]	3.6510(7)	3.5023	3.5172	7.0	15.6	16.4
Cg1···Cg2[v]	3.8770(7)	3.6524	3.6910	9.0	17.8	19.6

[a] Cg1, Cg2, Cg3, Cg4, Cg5 and Cg6 are the centroids of the rings S1/C11/C10/N1/C12, N2/N3/C21/C20/C13, O1/C1/C6/C7/C8/C9, C1-C6, C14-C19 and C22-C27, respectively. [b]Centroid distance between ring centroid I and J. [c]Vertical distance from ring centroid I to ring J. [d]Vertical distance from ring centroid J to ring I. [e]Dihedral angle between mean planes I and J. [f]Angle between the centroid vector Cg(I)···Cg(J) and the normal to the plane (I). [g]Angle between the centroid vector Cg(I)···Cg(J) and the normal to the plane (I). Symmetry codes: (i) -x,1-y,1-z; (ii) 1-x,1-y,-z; (iii) 1-x,-y,2-z; (iv) -x,-y,1-z; (v) 1-x,-y,-z.

3.2. Hirshfeld surface analysis

Hirshfeld surface analysis has been performed to identify and elucidate the contribution of significant intermolecular interactions observed in the crystal packing. The pattern of intermolecular contacts is similar in the three compounds, which prompted us to explore the contribution of weak non covalent interactions in the supramolecular assembly, as well as the importance of C-H···π and π···π stacking interactions in establishing the organization of the extended structure. Fig. 4 shows the Hirshfeld surfaces mapped over the d_{norm}, shape index and curvedness properties of compounds 1-3. The 2D fingerprint plots for 1-3 are shown in Fig. 5.

The two red regions labelled 1 in the d_{norm} map of **1** are attributed to weak C-H···Cl hydrogen bonds involving the acceptor Cl2 chlorine atom from one chorobenzene ring (Table 3). The pair of narrow pointed spikes labelled 1 around (d_e + d_i) of 2.7 Å in the fingerprint plot show the presence of H···Cl/Cl···H contacts which comprise 17.3% of total Hirshfeld surface area. The red spots located in the chlorobenzene (centroid Cg6) and in the 2H-chromen-2-one moiety (centroid Cg3) are attributed to π···π stacking interactions associated to Cg3···Cg6 contacts with a distance of 3.6838(3) Å. The Cg···Cg interactions described previously for **1** can be seen on the Hirshfeld surface mapped over shape index (Fig. 4, column 2), as a pattern of alternating red and blue triangles with suitable symmetry. In addition, the curvedness map (Figure 4, column 3) clearly shows large green regions at the same side of the molecule, evidencing π···π stacking interactions. The fingerprint plot of **1** (Fig. 5) also highlights the green area around d_e = d_i ~ 1.8 Å which corresponds to aryl-stacking interactions with 10.0% of contribution to the total Hirshfeld surface area. The H···S/S···H contacts attributed to weak C-H···S interactions can be seen as white regions in the d_{norm} surface, with 5.7% of contribution. The red areas labelled 4 in the d_{norm} map represent H···C/C···H contacts associated to C-H···π interactions. These C-H···π contacts are also evident from a pair of wings in the top left and button right region of the 2D fingerprint plots (Figure 5). The shape of the observed wings and the sum of d_e and d_i point out the importance of this interaction. The 2D fingerprint plot of **1** indicates that H···C/C···H contacts comprise 15.0% of the total Hirshfeld surface. The deep red spots labelled 3 in the d_{norm} map of compound **1** is attributed to lope pair···π interactions involving the O1 atom of the 2H-chromen-2-one moiety and the chlorobenzene ring (centroid Cg5), as was described previously.

The d_{norm} surface of compound **2** shows a small red spot labelled 1 attributed to weak C18-H18···O1 hydrogen bonds. These H···O/O···H contacts are visible in the 2D fingerprint plot as broad spikes labelled 2 and comprise 9.2% of total Hirshfeld surface area. The red spots labelled 2 in the d_{norm} map is an indicative of C-H···π interactions involving the H2 atom and the chlorobenzene ring (Cg5 centroid). These interactions are also visible in the fingerprint plots as a pair of wings at (d_e + d_i) ~ 3.1 Å contributing 12.6% to the total Hirshfeld surface area. The presence of π···π stacking interactions in compound **2** is confirmed by the two deep red spots labelled 3 in the d_{norm} map and by the appearance of red and blue triangles on the shape index surfaces identified as red circles in Figure 4, column 2. These interactions comprise 13.2% of the total Hirshfeld surface area.

The Hirshfeld surfaces of compound **3** mapped over d_{norm} function shows two deep red spots labelled 1 attributed to C11-H11···O1 hydrogen bonds and the red spot labelled 2 corresponds to C21-H21B···O1 hydrogen bonds, as was described previously. These contacts appeared as narrow pointed spikes at (d_e + d_i) ~ 1.75 Å in the fingerprint plots (Figure 5) contributing 9.5% of the total Hirshfeld surface. The red regions labelled 3 in the d_{norm} surface are assigned to π···π stacking interactions, as shown in shape index and curvedness surfaces. The H···H contacts have the most important contribution to the total Hirshfeld surface area with 29.3%, 38.9% and 42.4% for compounds **1**, **2** and **3**, respectively. These contacts are visible in the 2D fingerprint plots as middle scattered points and showed as two symmetrical broad regions.

View Article Online
DOI: 10.1039/D0NJ02931A

Journal Name

ARTICLE

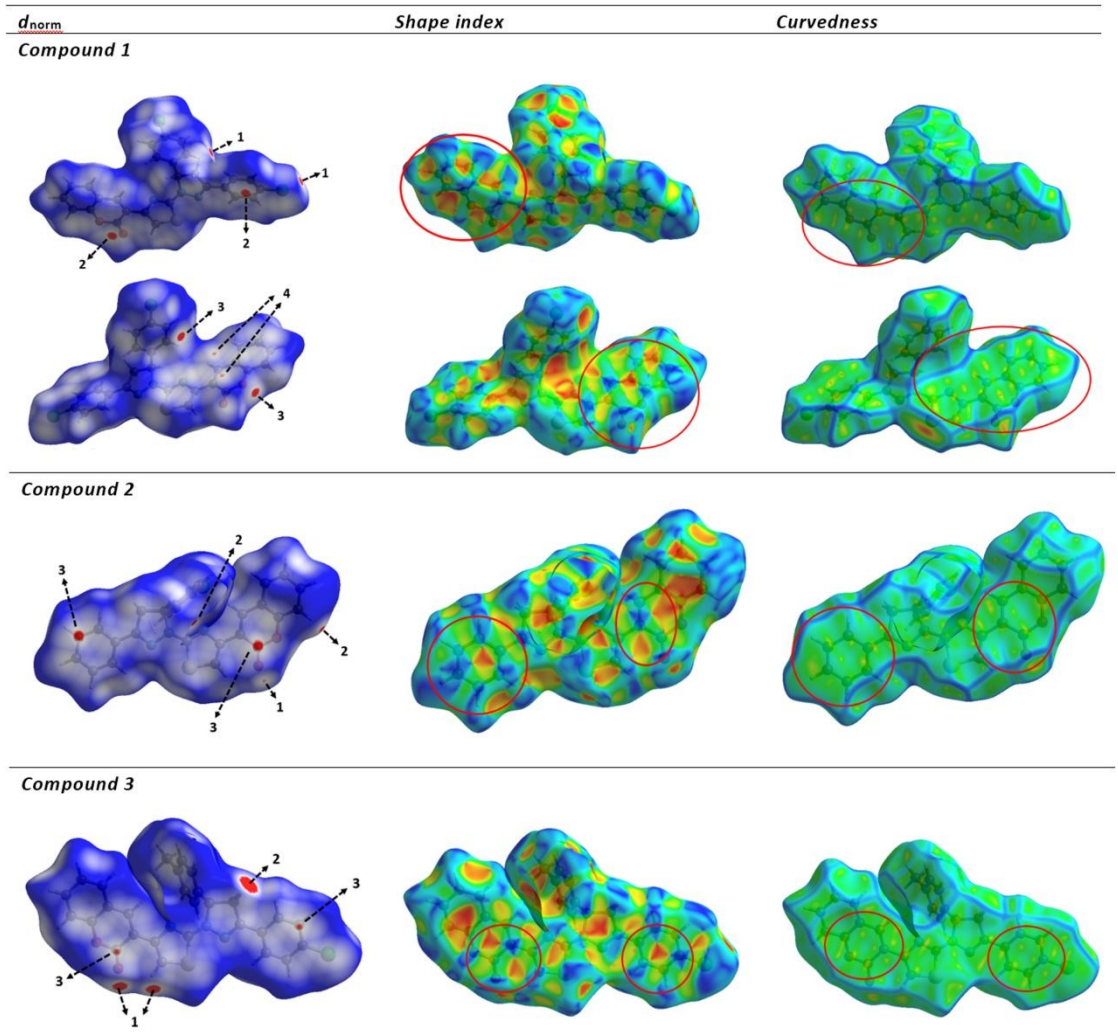

Fig. 4 Hirshfeld surfaces d_{norm}, shape index and curvedness for compounds **1**-**3**. Molecule **1** is shown in two different orientations. The numbered arrows are discussed in the main text.

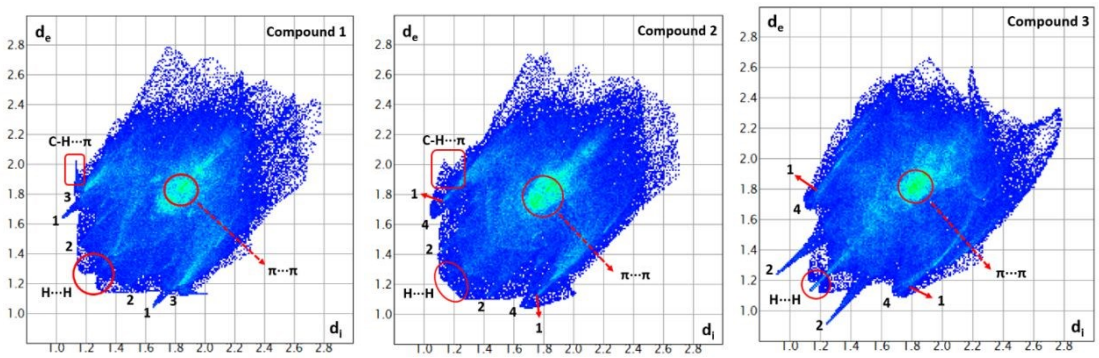

Fig. 5 2D fingerprint plots for compounds **1**-**3** showing: (1) H···Cl/Cl···H, (2) H···O/O···H, (3) H···S/S···H, (4) H···C/C···H contacts.

View Article Online
DOI: 10.1039/D0NJ02931A

Journal Name

ARTICLE

3.3. DFT study

The theoretical study is devoted to analyse the interesting supramolecular assemblies observed in compounds **1**–**3** governed by different types of π-stacking interactions in combination with C–H···π interactions. The existence of a variety of heteroaromatic rings in these compounds facilitates the formation several types of π–π stacking interactions, including the nonaromatic 4,5-dihydropyrazole ring. First of all, we have computed the molecular electrostatic potential surface of compound **1** as a model of the three compounds, that is shown in Fig. 6. The MEP minimum (most negative) is located at the O-atom of the coumarine ring (–40 kcal/mol) and the most positive values at the H-atoms of the 4,5-dihydropyrazole ring. Interestingly, the surface also reveals that the MEP values over the coumarin ring are of opposite sign, thus anticipating a strong tendency to form antiparallel π-stacking interactions to maximize attractive electrostatic forces. The same occurs with the adjacent thiazole and 4,5-dihydropyrazole ring that exhibit negative and positive MEP values over the centre of the rings. Finally, the MEP values are negative over the chlorophenyl rings, thus supporting the formation of C–H···π interactions. It is also worthy to comment that the MEP values alternate from positive to negative in the different coplanar rings of compound **1**. This fact explains the tendency to form antiparallel displaced π–π assemblies as recurrent motifs in the solid state architecture of compounds **1**–**3**.

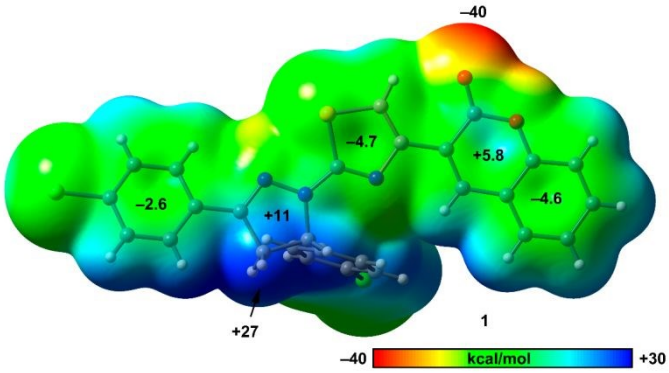

Fig. 6 MEP surface (0.001 a.u. isosurface) of compound **1** at the M06-2X-D3/def2-TZVP level of theory. The energies at selected points of the surface are indicated in kcal/mol.

Fig. 7a shows a partial view of the X-ray structure of **1** focusing on the π-stacking. It can be observed the formation of two different π–π stacking modes. In the denoted as $(\pi–\pi)_1$ (see Fig. 7b), the chlorophenyl and the lactone rings of both ends are stacked in addition to the formation of an antiparallel arrangement of the 4,5-dihydropyrazolylthiazole moieties. This binding mode strongly agrees with the MEP surface analysis, since the positive part (π-acidic) of coumarine interacts with the negative (π-basic) chlorophenyl ring and also the positive 4,5-dihydropyrazole is stacked with the negative thiazole ring. It is worthy to mention that exactly the same motif is found in compounds **2** (see Fig. 8a,b) and **3** (see Fig. 9a,b). In fact, the interactions energies are large, negative and similar for the three compounds, ranging from –22.6 to –22.7 kcal/mol, thus confirming the importance of this motif in the solid state of the three compounds. This large interaction energy is due to the large overlap of the π-systems and the perfect combination of π-acidic···π-basic interactions (electrostatically enhanced π–π stacking). It is also interesting to highlight the unconventional stacking of the 4,5-dihydropyrazole···thiazole moieties since it involves a partial aliphatic ring. In the other binding mode, denoted as $(\pi–\pi)_2$ (see Fig. 7c), the coumarine rings form an antiparallel electrostatically enhanced π–π stacking interactions, also in good agreement with the MEP surface analysis. Moreover, the π–π stacking interaction between the thiazole ring and the coumarine is significantly displaced to avoid the electrostatic repulsion between the negative rings. In fact, the geometry of this stacking mode is clearly influenced by the formation of two short C–H···π interactions (2.84 Å). The interaction energy of $(\pi–\pi)_2$ binding mode in **1** is ΔE_2 = –23.3 kcal/mol, very similar to that of $(\pi–\pi)_1$, thus revealing that both binding modes are equally important. Compounds **2** and **3** (see Figs. 8c and 9c, respectively) also present very similar arrangements and binding energies, thus confirming the relevance of this motif. The main difference is that in compound **3** the dimerization energy for the $(\pi–\pi)_2$ binding mode is weaker that likely due to the longer C–H···π interaction (3.04 Å) observed for this compound.

To further characterize both π–π stacking modes described above, "non-covalent Interaction plot" (NCI plot) index has been used in both dimers of compound **1** as representative example. The NCI plot is an intuitive visualization index that facilitates the visualization and characterization of non-covalent interactions and clearly shows which molecular regions interact. The colour scheme is a red-yellow-green-blue scale with red (repulsive) and blue (attractive). Yellow and green surfaces correspond to weak repulsive and weak attractive interactions, respectively. The NCI plot isosurfaces of both dimers of compound **1** are shown in Fig. 10 using two different orientations (perspective and on-top). The on-top representation of the $(\pi–\pi)_1$ stacking mode confirms the large overlap of the π-systems since the green isosurface extends from one end to the other of the conjugated system.

View Article Online
DOI: 10.1039/D0NJ02931A

Journal Name

ARTICLE

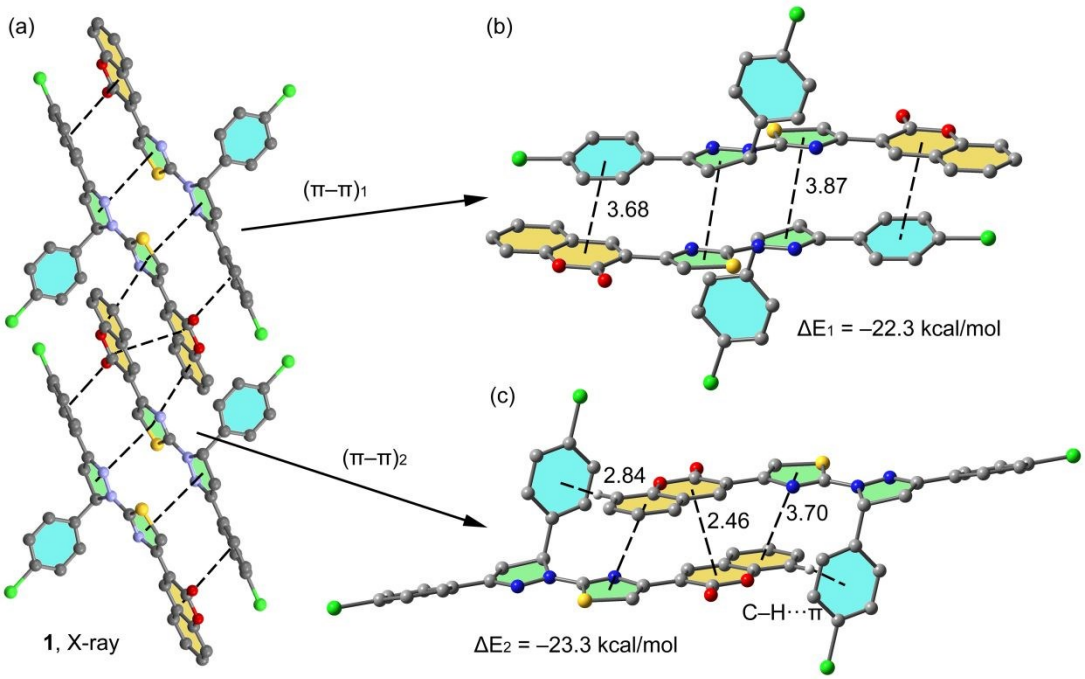

Fig. 7 (a) Partial view of the X-ray structure of **1**. (b,c) Theoretical models used to evaluate the dimerization energies at the M06-2x-D3/def2-TZVP level of theory. Distances in Å. H-atoms omitted for clarity apart from those participating in the C–H···π interaction

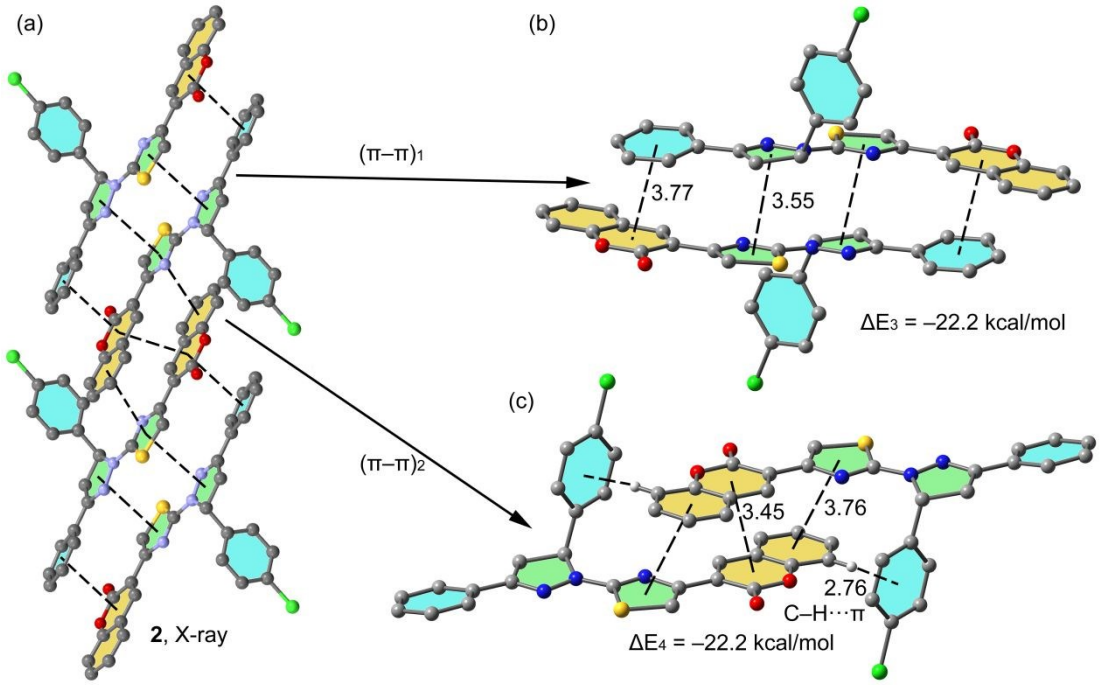

Fig. 8 (a) Partial view of the X-ray structure of **2**. (b,c) Theoretical models used to evaluate the dimerization energies at the M06-2x-D3/def2-TZVP level of theory. Distances in Å. H-atoms omitted for clarity apart from those participating in the C–H···π interaction

View Article Online
DOI: 10.1039/D0NJ02931A

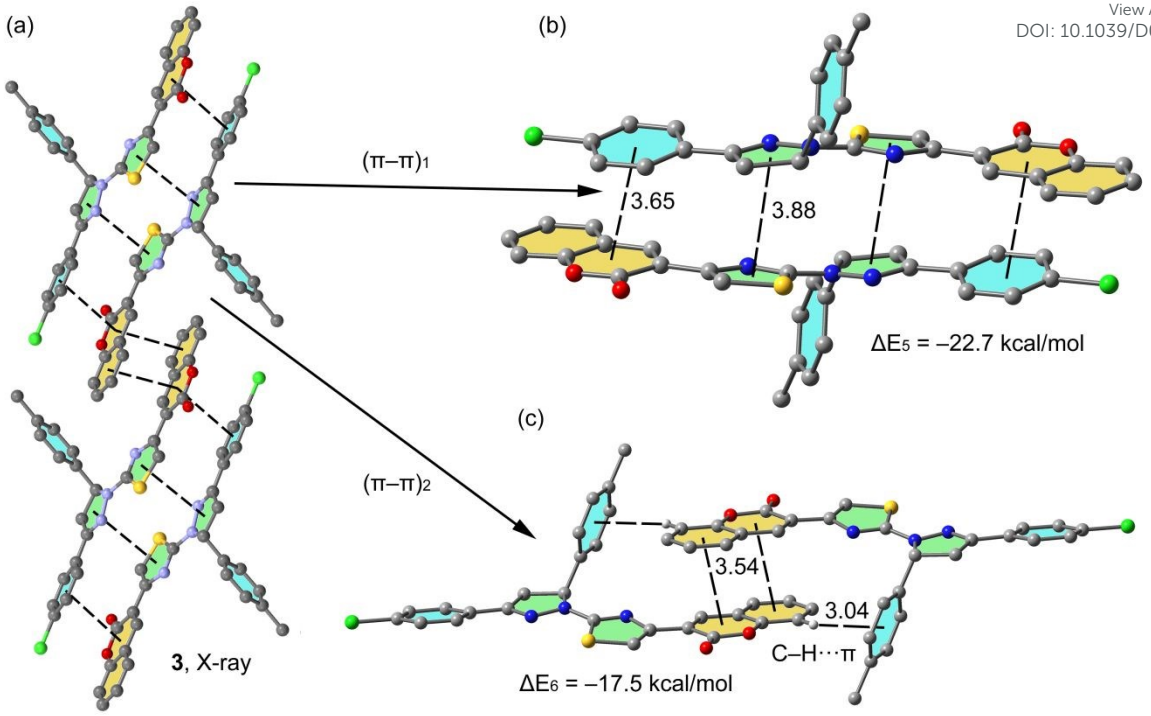

Fig. 9 (a) Partial view of the X-ray structure of **3**. (b,c) Theoretical models used to evaluate the dimerization energies at the M06-2x-D3/def2-TZVP level of theory. Distances in Å. H-atoms omitted for clarity apart from those participating in the C–H···π interaction

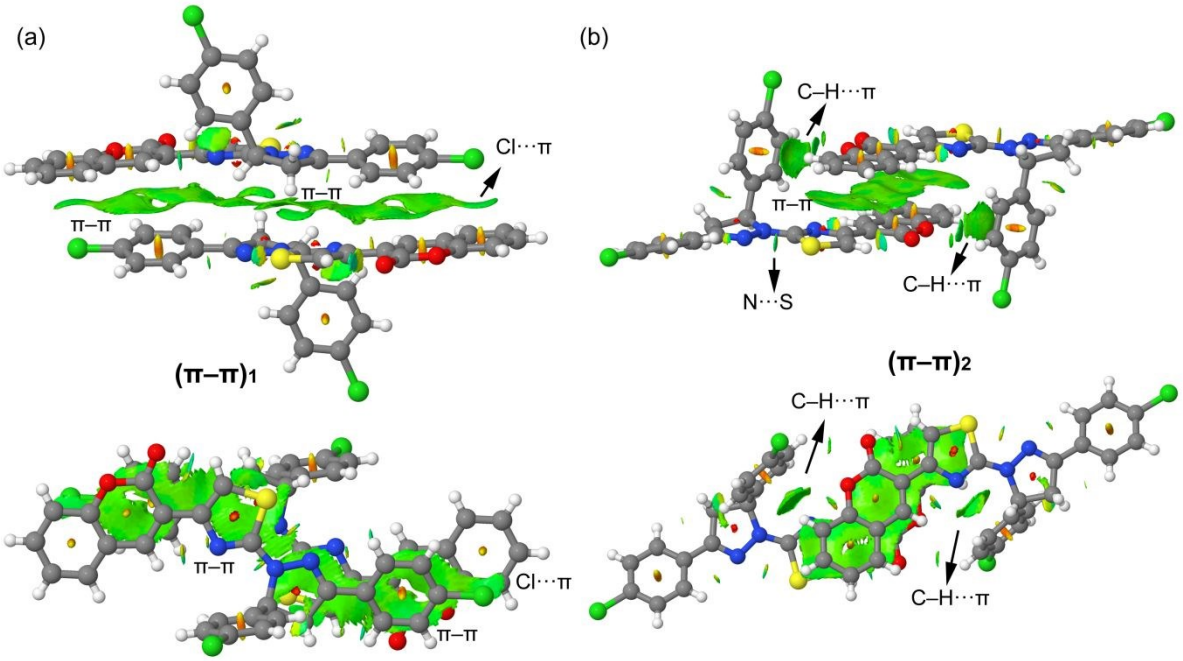

Fig. 10 NCI surface of the $(\pi–\pi)_1$ (a) and $(\pi–\pi)_2$ (b) stacking modes in compound **1**, using perspective and on-top views The gradient cut-off is s = 0.35 au, and the colour scale is $-0.04 < \rho < 0.04$ au.

Moreover, the NCIplot also shows that the Cl-atom of the p-chlorophenyl ring also participates in the binding mechanism (Cl···π). It is also interesting to highlight that in the p-chlorophenyl···coumarine stacking, only the lactone ring participates in the interaction (see Fig. 10a, on-top representation), in sharp agreement with the MEP surface analysis commented above. The NCIplot representation of the $(\pi–\pi)_2$ stacking mode (see Fig. 10b) also shows a large and green isosurface that characterizes the antiparallel π–π stacking of the coumarine rings, which also extends to the displaced thiazole rings. Moreover, two symmetrically equivalent green isosurfaces are located between the perpendicular chlorophenyl rings and the aromatic H-atoms, thus confirming the existence of the C–H···π interactions.

These isosurfaces almost embrace the whole aromatic ring, thus confirming the importance and energetic relevance of the C–H···π interactions in the stabilization of this assembly. Finally, the NCIplot also shows the existence of a small isosurface located between the S and N groups of the thiazole and 4,5-dihydropyrazole rings, respectively. Therefore, an interesting chalcogen bond also contributes to the planarity of the 4,5-dihydropyrazolylthiazole moiety.

4. Concluding remarks

Three new 4,5-dihydropyrazolylthiazole-coumarin hybrids have been synthesized and X-ray characterized that present recurrent π–π stacking motifs, which have been studied by means of Hirshfeld surface analysis and DFT calculations. The energetic study reveals that both π-stacking motifs present very strong interaction energies because the antiparallel arrangement of the π-systems that facilitates the formation of electrostatically enhanced π–π staking interactions, as demonstrated by the MEP surface analysis. The NCIPlot confirmed the strong complementarity of the π systems and the relevance of the C–H···π interactions in one of both π–π staking modes. Finally, it is interesting to highlight the behaviour of the 4,5-dihydropyrazolylthiazole fragments where the aliphatic ring stacks over the aromatic one and vice versa to maximize the electrostatic attraction. To our knowledge, this type of stacking involving heteroaliphatic and heteroaromatic five membered rings is unprecedented. Future directions of this work include fluorescence experiments to investigate whether pyrazol-thiazol fragments quench the expected coumparin-centered emission.

Acknowledgments

Authors are thankful to Quaid-i-Azam University Islamabad, Pakistan for financial support. We thank the MICIU/AEI (project CTQ2017-85821-R FEDER funds) for financial support. We thank the CTI (UIB) for computational facilities.

Conflicts of interest

The authors declare no conflicts of interest

References

1. K. Z. Laczkowski, A. Biernasiuk, A. Baranowska-Laczkowska, K. Misiura, A. Malm, T. Plech and A. Paneth, *Med. Chem*., 2016, **12**, 553-562.
2. I. P. Singh, S. Gupta and S. Kumar, *Med. Chem*., 2020, **16**, 4-23.
3. Z. A Muhammad, G. S Masaret, M. M. Amin, M. A. Abdallah and T. A Farghaly, *Med. Chem*., 2017, **13**, 226-238.
4. C. I. Lino, I. G. de Souza, B. M. Borelli, T. T. S. Matos, I. N. S. Teixeira, J. P. Ramos, E. M. de Souza Fagundes, P. de Oliveira Fernandes, V. G. Maltarollo and S. Johann, *Eur. J. Med. Chem*., 2018, **151**, 248-260.
5. Y. K. Abhale, A. Shinde, K. K. Deshmukh, L. Nawale, D. Sarkar and P. C. Mhaske, *Med. Chem. Res*., 2017, 26, 2557-2567.
6. Y. Lu, C.-M. Li, Z. Wang, C. R. Ross, J. Chen, J. T. Dalton, W. Li and D. D. Miller, *J. Med. Chem*., 2009, **52**, 1701-1711.
7. M. Madni, S. Hameed, M. N. Ahmed, M. N. Tahir, N. A. Al-Masoudi and C. Pannecouque, *Med. Chem. Res*., 2017, **26**, 2653-2665.
8. O. S. Afifi, O. G. Shaaban, H. A. A. El Razik, S. E.-D. A. S. El, F. A. Ashour, A. A. El-Tombary and M. M. Abu-Serie, *Bioorg. Chem*., 2019, **87**, 821-837.
9. O. I. El-Sabbagh, M. M. Baraka, S. M. Ibrahim, C. Pannecouque, G. Andrei, R. Snoeck, J. Balzarini and A. A. Rashad, *Eur. J. Med. Chem*., 2009, **44**, 3746-3753.
10. F. Jorquera, M. Almar, A. Jimeno, M. Gonzalez-Sastre and J. Gonzalez-Gallego, *J. Pharm. Biomed. Anal*., 1995, **13**, 1141-1145.
11. A. K. Tewari, P. Srivastava, V. P. Singh, A. Singh, R. K. Goel and C. G. Mohan, *Chem. Pharm. Bull*., 2010, **58**, 634-638.
12. M. M. Edrees, S. A. Melha, A. M. Saad, N. A. Kheder, S. M. Gomha and Z. A. Muhammad, *Molecules*, 2018, 23, 2970.
13. Shubhalaxmi, L. Pathak, K. Ananda and K. S. Bhat, *Cogent Chemistry*, 2016, **2**, 1141388.
14. P. S. Mahajan, M. D. Nikam, A. V. Chate, A. S. Bobade and C. H. Gill, *J. Heterocycl. Chem*., 2017, **54**, 44-50.
15. Y. R. Prasad, A. L. Rao, L. Prasoona, K. Murali and P. R. Kumar, Bioorg. *Med. Chem. Lett*., 2005, **15**, 5030-5034.
16. A. Kamal, K. S. Reddy, M. N. A. Khan, R. V. Shetti, M. J. Ramaiah, S. Pushpavalli, C. Srinivas, M. Pal-Bhadra, M. Chourasia and G. N. Sastry, *Biorg. Med. Chem*., 2010, **18**, 4747-4761.
17. F. Azam, B. A. El-gnidi, I. A. Alkskas and M. A. Ahmed, *J. Enzyme Inhib. Med. Chem*., 2010, **25**, 818-826.
18. R. N. Sharma, F. P. Xavier, K. K. Vasu, S. C. Chaturvedi and S. S. Pancholi, *J. Enzyme Inhib. Med. Chem*., 2009, **24**, 890-897.
19. I. Kostova, S. Raleva, P. Genova and R. Argirova, *Bioinorg. Chem. Appl*., 2006, **2006**, 68274.
20. C. Spino, M. Dodier and S. Sotheeswaran, *Bioorg. Med. Chem. Lett*., 1998, **8**, 3475-3478.
21. M. Mohammadi-Khanaposhtani, N. Ahangar, S. Sobhani, P. H. Masihi, A. Shakiba, M. Saeedi and T. Akbarzadeh, *Bioorg. Chem*., 2019, **89**, 102989.
22. R. Kenchappa, Y. D. Bodke, A. Chandrashekar, M. A. Sindhe and S. Peethambar, *Arab. J. Chem*., 2017, **10**, S3895-S3906.
23. J. Yu, L. Wang, R. L. Walzem, E. G. Miller, L. M. Pike and B. S. Patil, *J. Agric. Food. Chem*., 2005, **53**, 2009-2014.
24. S. Sardari, Y. Mori, K. Horita, R. G. Micetich, S. Nishibe and M. Daneshtalab, *Biorg. Med. Chem*., 1999, **7**, 1933-1940.
25. A. Thakur, R. Singla and V. Jaitak, *Eur. J. Med. Chem*., 2015, **101**, 476-495.
26. M. Madni, M. N. Ahmed, S. Hameed, S. W. A. Shah, U. Rashid, K. Ayub, M. N. Tahir and T. Mahmood, *J. Mol. Struct*., 2018, **1168**, 175-186.
27. S. Ben Mohamed, Y. Rachedi, M. Hamdi, F. Le Bideau, C. Dejean and F. Dumas, *Eur. J. Org. Chem*., 2016, 2628-2636.
28. (a) K. Vaarla, R. K. Kesharwani, K. Santosh, R. R. Vedula, S. Kotamraju and M. K. Toopurani, *Bioorg. Med. Chem. Lett*., 2015, **25**, 5797-5803; (b) X. Yu, D. Scheller, O. Rademacher and T. Wolff, *J. Org. Chem*., 2003, **68**, 7386-7399.
29. (a) A. Al-Kawkabani, M. Makhloufi-Chebli, N. Benosmane, B. Boutemeur-Kheddis, M. Hamdi and A. M. Silva, *J. Mol. Struct*., 2017, **1146**, 285-291; (b) H. N. Harishkumar, K. M. Mahadevan and J. N. Masagalli, S. *Afr. J. Chem*., 2012, **65**, 5-9.
30. S. H. Mashraqui, H. Mistry and S. Sundaram, *J. Heterocycl. Chem*., 2006, **43**, 917-923.
31. X. Li, Y. Zhao, T. Wang, M. Shi and F. Wu, *Dyes and Pigments*, 2007, **74**, 108-112.
32. K.-L. An, K. H. Park and K. Jun, *Bull. Korean Chem. Soc*., 2014, **35**, 2183-2185.
33. (a) H. G. Bonacorso, M. B. Rodrigues, W. C. Rosa, L. B. Silva, C. P. Frizzo, N. Zanatta and M. A. Martins, *J. Fluorine Chem*., 2015, **178**, 296-305; (b) D. P. Specht, P. A. Martic and S. Farid, *Tetrahedron*, 1982, **38**, 1203-1211.

34. M. N. Ahmed, M. Arif, F. Jabeen, H. A. Khan, K. A. Yasin, M. N. Tahir, A. Franconetti and A. Frontera, *New J. Chem*., 2019, **43**, 8122-8131.
35. M. N. Ahmed, K. Y. Ansar, S. Aziz, S. Khan, M. N. Tahir, D. M. Gil and A. Frontera, *CrystEngComm*, 2020, **22**, 3567-3578.
36. (a) (a) J. W. G. Bloom and S. E. Wheeler, *Angew. Chem. Int. Ed*., 2011, **50**, 7847–7849; (b) S. Grimme, *Angew. Chem. Int. Ed*., 2008, **47**, 3430–3434.
37. (a) E. R. T. Tiekink, *Chem. Commun*., 2014, 50**,** 11079–11082; (b) D. P. Malenov, D. B. Ninković, D. N. Sredojević and S. D. Zarić, *ChemPhysChem*, 2014, **15**, 2458 —2461; (c) Z. D. Tomić, V. M. Leovac, S. V. Pokorni, D. Zobel and S. D. Zarić, *Eur. J. Inorg. Chem*., 2003, 1222–1226; (d) D. N. Sredojević, Z. D. Tomić and S. D. Zarić, *Cryst. Growth Des*., 2010, **10**, 3901–3908; (e) A. Castineiras, A. G. Sicilia-Zafra, J. M. Gonzalez-Perez, D. Choquesillo-Lazarte and J. Niclos-Gutierrez, *Inorg. Chem*., 2002, **41**, 6956–6958; (f) K. F. Konidaris, C. N. Morrison, J. G. Servetas, M. Haukka, Y. Lan, A. K. Powell, J. C. Plakatouras and G. E. Kostakis, *CrystEngComm*, 2012, **14**, 1842–1849
38. (a) H. H. Monfared, M. Vahedpour, M. M. Yeganeh, M. Ghorbanloo, P. Mayer and C. Janiak, *Dalton Trans*., 2011, **40**, 1286–1294; (b) J. P. Blagojević and S. D. Zarić, *Chem. Commun*., 2015, **51**, 12989–12991; (c) J. Ran and M. W. Wong, *J. Phys. Chem. A*, 2006, **110**, 9702–9709.
39. D. B. Ninković, D. Z. Vojislavljević-Vasilev, V. B. Medaković, M. B. Hall, E. N. Brothers and S. D. Zarić, *Phys. Chem. Chem. Phys*., 2016, **18**, 25791-25795
40. K. S. Kim, S. Karthikeyan and N. J. Singh, *J. Chem. Theory Comput*., 2011, **7**, 3471–3477
41. (a) M. Madni, S. Hameed, M. N. Ahmed, K. A. Yasin and M. N. Tahir, *Chinese J. Struct. Chem*., 2015, **7**, 1013-1018; (b) Y.-M. Lin, Y. Zhou, M. T. Flavin, L.-M. Zhou, W. Nie and F.-C. Chen, *Biorg. Med. Chem*., 2002, **10**, 2795-2802; (c) B. F. Abdel-Wahab, H. A. Abdel-Aziz and E. M. Ahmed, *Eur. J. Med. Chem*., 2009, **44**, 2632-2635.
42. A. Bruker, Bruker AXS Inc., Madison, Wisconsin, USA, 2009.
43. G. M. Sheldrick, *Acta Cryst*., 2008, **A64**, 112-122.
44. G. M. Sheldrick, *Acta Cryst*., 2015, **C71**, 3-8.
45. L. J. Farrugia, *J. Appl. Crystallogr*., 2012, **45**, 849-854.
46. S. Bruker, Inc., Madison, Wisconsin, USA, 2013.
47. J. J. McKinnon, M. A. Spackman and A. S. Mitchell, *Acta Cryst*., 2004, **B60**, 627-668.
48. Y.-H. Luo, C. Chen, D.-L. Hong, X.-T. He, J.-W. Wang and B.-W. Sun, *J. Phys. Chem. Lett*., 2018, **9**, 2158-2163.
49. J. J. McKinnon, D. Jayatilaka and M. A. Spackman, *Chem. Commun*., 2007, 3814-3816.
50. M. A. Spackman and D. Jayatilaka, *CrystEngComm*, 2009, **11**, 19-32.
51. M. Spackman, *Chem. Rev*., 1992, **92**, 1769-1797.
52. M. Turner, J. McKinnon, S. Wolff, D. Grimwood, P. Spackman, D. Jayatilaka and M. Spackman, The University of Western Australia Perth, WA, Australia, 2017.
53. A. Parkin, G. Barr, W. Dong, C. J. Gilmore, D. Jayatilaka, J. J. McKinnon, M. A. Spackman and C. C. Wilson, *CrystEngComm*, 2007, **9**, 648-652.
54. S. B. Boys and F. Bernardi, Mol. Phys. 1970, 19, 553-566.
55. R. Ahlrichs, M. Bär, M. Häser, H. Horn and C. Kölmel, *Chem. Phys. Lett*., 1989, **162**, 165-169.
56. Y. Zhao and D.G. Truhlar, *Theor. Chem. Acc*., 2006, **120**, 215–241.
57. S. Grimme, J. Antony, S. Ehrlich and H. Krieg, *J. Chem. Phys*., 2010, **132**, 154104.
58. (a) F. Weigend and R. Ahlrichs, *Phys. Chem. Chem. Phys*., 2005, **7**, 3297-3305; (b) F. Weigend, *Phys. Chem. Chem. Phys*., 2006, **8**, 1057-1065.
59. (a) P. Manna, S. K. Seth, M. Mitra, S. R. Choudhury, A Bauzá, A Frontera and S. Mukhopadhyay, *Cryst. Growth Des*., 2014, **14**, 5812-5821 (b) M Mirzaei, H. Eshtiagh-Hosseini, Z. Bolouri, Z. Rahmati, A. Esmaeilzadeh, A. Hassanpoor, A. Bauza, P. Ballester, M. Barcelo-Oliver, J. T Mague, B. Notash and A. Frontera, *Cryst. Growth Des*., 2015, **15**, 1351-1361.
60. (a) J. Contreras-García, E. R. Johnson, S. Keinan, R. Chaudret, J.-P. Piquemal, D. N. Beratan and W. Yang, *J Chem Theory Comput*., 2011, **7**, 625-632; (b) E. R. Johnson, S. Keinan, P. Mori-Sánchez, J. Contreras-García, A. J. Cohen and W. Yang, *J. Am. Chem. Soc*., 2010, **132**, 6498-6506.

DOI: 10.1039/D0NJ02931A

Two different π–π stacking modes are described, studied and characterized in the crystal structures of 4,5-dihydropyrazolyl-thiazole-coumarine hybrids, including a partial aliphatic ring.